

## Generation, evolution and breakdown of helical vortex wakes

A. Nemes<sup>1</sup>, M. Sherry<sup>1</sup>, D. Lo Jacono<sup>1,2,3</sup>, H. M. Blackburn<sup>4</sup> and J. Sheridan<sup>1</sup>

<sup>1</sup>FLAIR, Department of Mechanical and Aerospace Engineering  
Monash University, Melbourne, Victoria 3800, Australia

<sup>2</sup>Université de Toulouse; INPT, UPS; IMFT;  
All e Camille Soula, F-31400 Toulouse, France

<sup>3</sup>CNRS; IMFT; F-31400 Toulouse, France

<sup>4</sup>Department of Mechanical and Aerospace Engineering  
Monash University, Melbourne, Victoria 3800, Australia

### Abstract

A study of the wake behind a Glauert model rotor in a water channel is reported. Phase-locked planar PIV is used to extract signatures of the coherent structures in the wake. The results show for first time both the tip and root vortices behind a wind turbine model operating at the run-away condition. Features of the wake are reported and evolution of the vortical filaments are discussed.

### Introduction

Understanding the dynamics of the wake behind a horizontal-axis wind turbine (HAWT) is important due to its influences on wind farm performance, fatigue and noise [11]. The wake is characterised by the velocity deficit relating to the energy extracted by the turbine and vortices shed into the wake that are generated by the rotating blades. These coherent vortical structures comprise of counter-rotating tip and root vortices shed by each blade which follow helical paths downstream. The evolution and breakdown of the vortices also has a strong influence on the characteristics of the wake far downstream of the rotor [2]. In wind farm arrangements the wind direction can result in turbines being subjected to the wake of upstream turbines, leading to a drop in the performance and potential fatigue loading. The dynamics of the helical vortex evolution is of interest not just to the wind energy industry, but also the aviation and marine industries where helicopters, airplane and marine propellers generate similar coherent structures. The influence of these wake structures in a range of applications has motivated studies into the stability of helical vortices in various configurations.

Early studies [13] provided the theoretical framework for inviscid linear stability analysis of helical vortex filaments and showed that they are prone to three general modes of instability: a short-wave, a long-wave and a mutual inductance mode whereby subsequent axial turns of the helices interact according to the Biot-Savart law. Results indicate the instability modes are independent of the perturbation source. Numerous theoretical studies followed which analysed the stability of tip helices in configurations of  $N$  helical vortices, with and without accompanying counter-rotating root vortices or a single hub vortex [8, 14]. They show that the presence of root and hub vortices results in inherently unstable tip vortices, however experimental and numerical studies [7, 12] have recorded the tip vortices persisting for multiple rotor diameters downstream [1] prior to undergoing mutual inductance, which results in entanglement and coalescence of the vortices [3].

Recent experiments [5] have provided new depths of insight into the instability mechanisms of a marine propeller, a rotor system with helical tip vortices and an axial hub vortex. The results

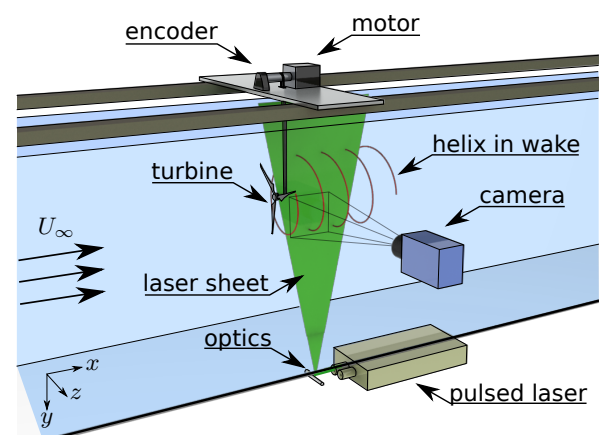


Figure 1: Schematic of the experimental setup. The simulated pathline of a tip vortex shown as it intersects the measurement plane illuminated by the laser.

show the presence of both shortwave and mutual inductance modes and conclude the initiation of the tip vortex instability is a result of instability initiated in the axial hub vortex. The wake of a marine propeller is different due to the energy addition of the rotor to the flow and a single hub vortex as opposed to individual root vortices. The current set of experiments investigates the tip and root vortices in the wake of a 3 bladed wind turbine. Evolution of the vortex paths is presented through a phase-locked PIV analysis.

### Experimental setup

Experiments were conducted in the free-surface recirculating water channel of FLAIR in the Department of Mechanical and Aerospace Engineering at Monash University. The water channel facility has a test section of 4000 mm in length, 600 mm in width, and 800 mm in depth. The freestream velocity,  $U_\infty$ , was maintained at  $200 \text{ mms}^{-1}$  and the water temperature was monitored during acquisition and varied by less than  $T = 0.1^\circ \text{C}$ .

Particle image velocimetry (PIV) was used to reconstruct 2D velocity fields behind the turbine. The flow was seeded with hollow microspheres (Spherical 110P8, Potters Industries Inc.) with a nominal diameter of  $13 \mu\text{m}$  and a specific weight of  $1.1 \text{ gcm}^{-3}$ .

Two miniature Nd:YAG pulsed lasers (Minilite II Q-Switched lasers, Continuum) produced a 2 mm thick planar sheet illuminating the particles in a vertical streamwise plane intersecting the turbine axis. A CCD camera (pco.4000, PCO AG) with

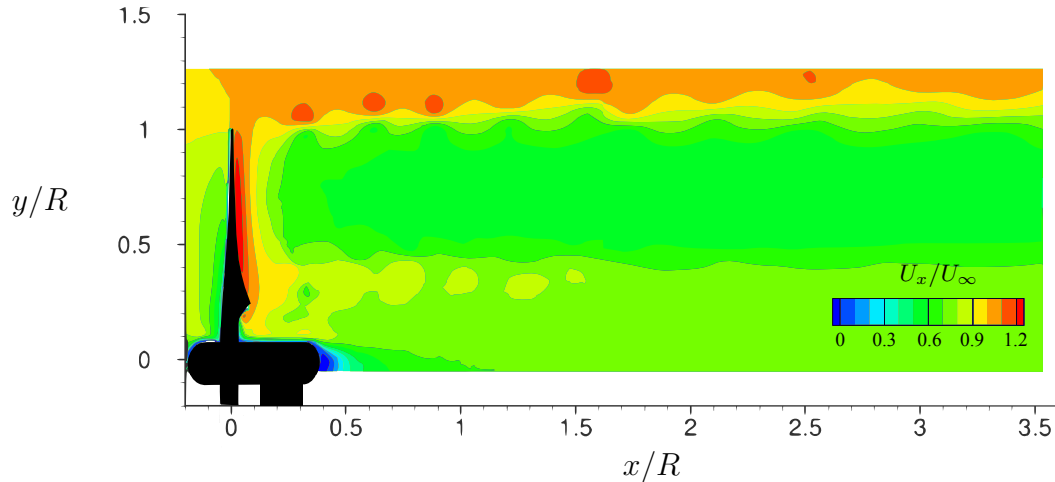


Figure 2: Streamwise velocity contours of the wake of the rotor at a runaway tip speed ratio of  $\lambda_R = 6.07$ .  $U_\infty$  is from left to right. The velocity gradients highlight the shear layer at the wake edge, while internally the signature velocity variation confirms the presence of root vortices.

4008 × 2672 pixel resolution and equipped with a 105 mm lens (AF105 Nikkor, Nikon Corporation) captured image pairs of the illuminated plane. In-house cross-correlation software [6] generated the instantaneous velocity field,  $(U, V)$ , from image pairs using  $32 \times 32$  pixel interrogation windows with 50% overlap to give a vector spacing resolution of  $8.2 \times 10^{-3}R$ . These fields were used to calculate the phase-locked out-of-plane vorticity ( $\omega_z$ ) fields. The experimental setup is shown in figure 1.

The three bladed optimum Glauert rotor used in the experiments was based on a NACA4412 airfoil and designed for low Reynolds number experiments. Consequently the operational tip speed ratio,  $\lambda_d = 3.5$ , is lower than that of full scale turbines ( $\approx 7$ ) given the aerodynamic performance of the airfoil at low  $Re$ . The blades profile was designed using the blade element momentum (BEM) and tip correction formulae of [9] was applied. The rotor blades have a radius of  $R = 115\text{mm}$ , and contain both twist and taper to minimise spanwise variations in blade loading ( $\Gamma_b = c(r)UC_L(r)$ ), where  $c(r)$ ,  $C_L(r)$  and  $U$  are the local blade chord, sectional lift coefficient and relative flow velocity respectively. The lifting surface purposely terminates outside the influence of the nacelle boundary layer to minimise effects of turbine support geometries on the root vortex formation [10].

The turbine was driven at the required tip speed ratio by a micro-stepping drive (OEM350–650 and 6K2 Controller, Parker). The drive shaft of the motor was situated above the water channel and a timing belt transferred the torque to the model turbine shaft through the tower support. An optical encoder (HBM5–1250, US Digital) attached to the drive shaft was used to monitor the turbine speed and blade position.

Measurements were taken on the centre plane of the wake, with a region of interest on the half of the wake that did not contain the support geometry. A three axis traverse (IMC–S8 controller, ISEL) was used to position the camera at multiple downstream locations to capture the wake evolution while maintaining a high spatial resolution of the vector fields. Phase-locked snapshots were taken at a single rotor position for each camera location providing a total of 800 statistically uncorrelated vector fields of the wake.

The model was investigated at a high tip speed ratio,  $\lambda_R = 6.07$ , nearing runaway conditions. The runaway tip speed ratio occurs in operational wind turbines when the generator load on the main shaft ceases, allowing the blades to spin freely — often with catastrophic consequences. The runaway tip speed ratio depends on the lift and drag properties of the airfoil. These

are crucial properties in the design of scaled wind turbine studies [10], especially when driving the turbine. Driving a turbine at too high a tip speed ratio will produce a propeller wake state rather than a wind turbine wake. In the runaway state, the net power (after friction) transferred to the blades by the fluid is balanced by the angular momentum contained in the tip and root vortices [4].

## Results

Figure 2 shows the phase-locked streamwise velocity contours,  $U_x$ , normalised by the freestream velocity,  $U_\infty$ . The field-of-view encompasses the top half of the wake (the half without the tower structure) from the blades to an axial distance of  $x/R = 3.5$  downstream. The freestream flow is from left to right with a blade and the turbine nacelle aligned with the 2D measurement plane. The rotating blade's tangential velocity vector is into the page. The velocity gradients highlight the wake velocity deficit and wake expansion, confirming the rotor is operating in a turbine state, and inferred low pressure wake. The distribution of the velocity deficit is near constant radially along the blade between  $0.4 < y/R < 1$ , highlighting good turbine performance. The deficit reduces slightly towards the wake centre-line. This distribution is dependent on the loading of the blades, and discussed further in relation to the vortex positions.

The phase average velocity field downstream of the rotor also captures the shear layer evolution between the wake and freestream. The velocity fluctuations relating to the coherent structures in the wake can be seen to retain the same phase spatially up to an axial distance  $x/R = 1.5$ .

### Helical vortex evolution

The near-wake vortex structures behind the turbine wake are presented in figure 3. Solid and dashed contours represent the clockwise (CW) positive and counter-clockwise (CCW) negative vorticity respectively. The tip and root vortices are clearly evident, represented by their phase-locked average out-of-plane vorticity component,  $\bar{\omega}_z$ , non-dimensionalised by  $U_\infty$  and  $R$ . Adjacent vortices are spaced at a vortex age ( $V_A$ ) of  $120^\circ$  apart due to the symmetry of the three bladed turbine, where vortex age ( $V_A$ ) is defined as the azimuthal travel of the blade since filament creation in degrees ( $^\circ$ ). These vorticity fields confirm experimentally for the first time the co-existence of tip and root vortices in a wind turbine wake prior to the onset of instabilities and breakdown.

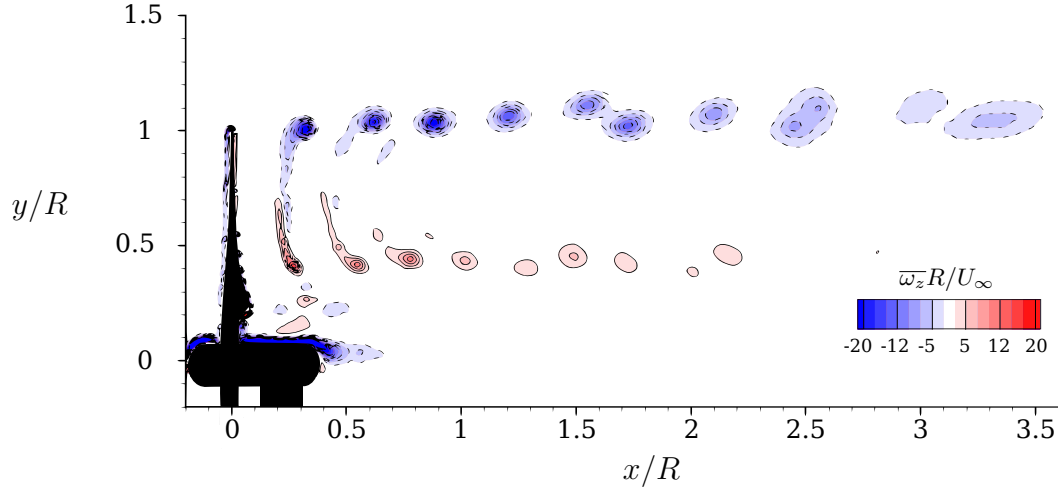


Figure 3: Vorticity contours of the wake of the rotor at a runaway tip speed ratio of  $\lambda_R = 6.07$ . Solid (dashed) contours of non-dimensionalised out-of-plane positive (negative) vorticity,  $\bar{\omega}_z R / U_\infty$  represent counter-clockwise (clockwise) rotation. Tip and root vortices are clearly visible in the wake and the roll-up and pairing of vortices is evident.

A pairing of the tip vortex helical filaments can be observed, becoming evident at  $x/R \geq 1.6$ . At this axial location the two interacting tip vortices have a vortex age of  $V_A = 600^\circ$  and  $720^\circ$ . The younger vortex ( $V_A = 600^\circ$ ) moves radially outward relative to the older vortex ( $V_A = 720^\circ$ ) due to the mutual induction between the two vortices. The corresponding root vortices can be seen to move in the opposite direction to the tip vortices, having opposite rotation, but undergo the same interaction. As the two interacting tip vortices advect further into the wake their entanglement evolves, with the filament core at  $V_A = 960^\circ$  overtaking the older vortex core of the other filament at  $V_A = 1080^\circ$ . These two filaments entangle further such that they appear as a single patch of vorticity at  $x/R \sim 3.3$  due to the phase-averaging of the vector fields. The vortex path is no longer steady due to the symmetry breakdown and results in spatial averaging of the out-of-plane vorticity scalar. Hence the tip vortex signature decreases rapidly thereafter. This pairing phenomenon has been seen experimentally in 2-bladed turbine visualisations [1]. The current study confirms the 3-bladed interaction, agreeing with prior visualisation of the wake behind a 3-bladed marine propeller [5]. Their propeller configuration differs in that it added energy to the flow and produced a single longitudinal hub vortex as opposed to distinct  $N$  root vortices. Upon the introduction of a perturbation into the system, inherent in the experimental nature of the study, any deviation from the helical symmetry results in the eventual entanglement of the filaments. The process here confirms that two of the three filaments experience a pairing, followed by the third filament coalescing with the entangled pair at which point the three are intertwined and undergo a complex vortex breakdown.

For the present results, the turbine is operating at a runaway tip speed ratio larger than the design tip speed ratio (*i.e.*  $\lambda_R \geq \lambda_d$ ) of the blade design, generating ‘off-design’ blade loading. This causes a radial circulation gradient outward of the root termination of the blade. The result is that the root vortices are shed into the wake at a radial distance of  $y/R = 0.4$ , and with no clear interaction between the root vortices and the nacelle boundary layer. Despite the three dimensional nature of the region immediately downstream of the nacelle, the wake centre-line is devoid of vorticity. This can be attributed to the planar experimental technique employed.

Blade wakes are visible at early vortex ages ( $V_A < 360^\circ$ ) in figure 3. These arise from the spanwise blade bound circulation gradients ( $d\Gamma_b/dr$ ) resulting in a vorticity sheet being shed from the trailing edge. In part, this can also be attributed to the ‘off-design’  $\lambda$ , at which uniform blade loading was desired.

Figure 3 shows that the tip and root vortices entrain vorticity from the blade wakes with the roll-up of the trailing vorticity sheet completed by  $V_A \leq 360^\circ$ . As the blade wakes are entrained into the helical vortex structures interaction with neighbouring vortices upstream is likely.

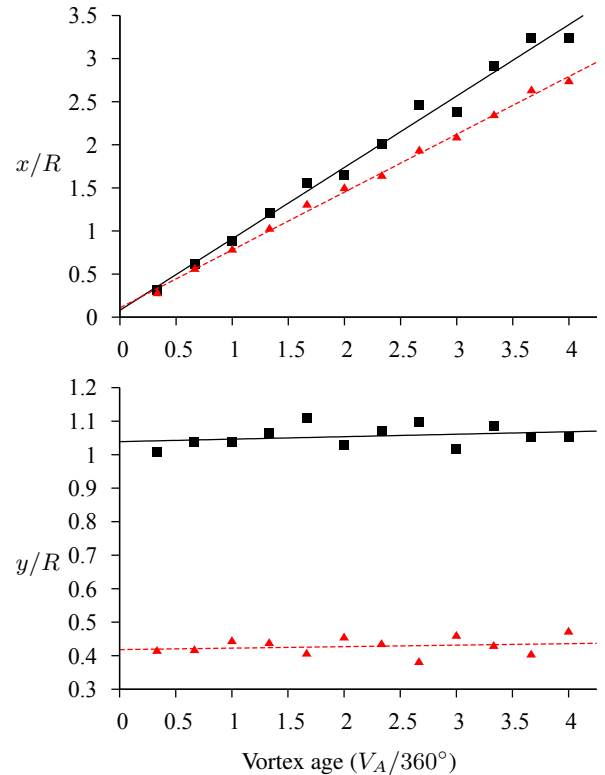


Figure 4: Axial (top) and radial (bottom) position of the tip and root vortices of a turbine at runaway ( $\lambda_R = 6.07$ ). Solid (dashed) lines/symbols represent tip (root) vortices. Mutual inductance can be observed affecting the axial location of the helical tip vortex from  $V_A > 720^\circ$ .

The trajectories of the tip and root vortices are shown in figure 4. The axial positions of the vortices have been fitted with a linear regression to obtain the helical pitch. For the tip vortices, the pitch is represented well by the linear regression at early ages, and can be seen to advect at a faster rate downstream than the

root vortices due to their proximity to the freestream flow. This axial separation between the tip and root vortices shed from the same blade increases with vortex age. At a axial distance of  $x/R \geq 1.5$  both tip and root vortices deviate from the helical pitch as the mutual induction between adjacent tip vortices alter their trajectories. From figure 3 it can be seen that every third vortex (relating to the same filament) undergoes the greatest deviation from the linear trend due to the mutual induction with its neighbour. The root vortices have a similar evolution with the same filament number experiencing the greatest deviation from the original helical pitch. The source of perturbation relating to the filaments that undergo pairing are likely introduced here through small inhomogeneities in the blade construction leading to variations in blade loading and hence vortex strengths. Further characterisation of the vortex properties and blade loading could shed insight into the genesis of the symmetry breakdown.

The radial position of the vortices are also represented in figure 4. The linear trends of the tip vortices see only a slight expansion of the wake, confirming the velocity contours that the turbine is close to a run-away condition. The pairing phenomenon induces a radial deviation in the tip and root vortices in opposite directions for the same cores.

### Conclusions

The wake behind a model turbine has been analysed with planar PIV. Although a highly three-dimensional flow, planar measurements have been shown to be able to capture the evolution of the helical vortices in the wake. Results confirm the vortex pairing of tip vortices, and have importantly captured for the first time the root vortices and their mutual interaction. This result provides avenues for examination of the dependence of the tip vortex interaction on the behaviour of the root vortices through manipulating their generation via input parameters. Importantly, it confirms that with appropriate blade design low Reynolds number model turbines can effectively generate helical vortex wakes.

### Acknowledgements

This work was supported by the Australian Research Council through Discovery Project DP1096444.

### References

- [1] Alfredsson, P. A. and Dahlberg, J. A., A preliminary wind tunnel study of windmill wake dispersion in various flow conditions, Technical report, The Aeronautical Research Institute of Sweden, 1979, aU-1499, part 7.
- [2] Barthelmie, R., Hansen, K., Frandsen, S., Rathmann, O., Schepers, J., Schlez, W., Phillips, J., Rados, K., Zervos, A., Politis, E. and Chaviaropoulos, P., Modelling and measuring flow and wind turbine wakes in large wind farms, *Wind Energy*, **12**, 2009, 431–444.
- [3] Bhagwat, M. and Leishman, J. G., Stability analysis of helicopter rotor wakes in axial flight, *Journal of the American Helicopter Society*, **45**, 2000, 165–178.
- [4] Ebert, P. R. and Wood, D. H., The near wake of a horizontal-axis wind turbine at runaway, *Renewable Energy*, **25**, 2002, 41–54.
- [5] Felli, M., Camussi, R. and Felice, F. D., Mechanisms of evolution of the propeller wake in the transition and far fields, *Journal of Fluid Mechanics*, **682**, 2011, 5–53.
- [6] Fouras, A., Lo Jacono, D. and Hourigan, K., Target free stereo piv: a novel technique with inherent error estimation and improved accuracy, *Experiments in Fluids*, **44**, 2008, 317–329.
- [7] Ivanell, S., Mikkelsen, R., Sørensen, J. and Henningson, D., Stability analysis of the tip vortices of a wind turbine, *Wind Energy*, **13**, 2010, 705–715.
- [8] Okulov, V. L. and Sørensen, J. N., Stability of helical tip vortices in a rotor far wake, *Journal of Fluid Mechanics*, **576**, 2007, 1–25.
- [9] Shen, W. Z., Mikkelsen, R. M., Sørensen, J. N. and Bak, C., Tip loss corrections for wind turbine computations, *Wind Energy*, **8**, 2005, 457–475.
- [10] Sherry, M., Sheridan, J. and Lo Jacono, D., Characterisation of a horizontal axis wind turbine's tip and root vortices, *Experiments in Fluids*, *Under review*.
- [11] Sørensen, J. N., Instability of helical tip vortices in rotor wakes, *Journal of Fluid Mechanics*, **682**, 2011, 1–4.
- [12] Walther, J. H., Guenot, M., Machefaux, E., Rasmussen, J. T., Chatelain, P., Okulov, V. L., Sørensen, J. N., Bergdorf, M. and Koumoutsakos, P., A numerical study of the stability of helical vortices using vortex methods, in *Journal of Physics: Conference Series*, 2007, volume 75, 012034, 012034.
- [13] Widnall, S., The stability of a helical vortex filament, *Journal of Fluid Mechanics*, **54**, 1972, 641–663.
- [14] Wood, D. H. and Boersma, J., On the motion of multiple helical vortices, *Journal of Fluid Mechanics*, **447**, 2001, 149–171.